Science of the Total Environment 747 (2020) 141214

Contents lists available at ScienceDirect

Science of the Total Environment

journal homepage: www.elsevier.com/locate/scitotenv

Sea-level rise will reduce net CO_2 uptake in subtropical coastal marshes

Ya-Lei Li [a,1], Hai-Qiang Guo [b,1], Zhen-Ming Ge [a,c,*], Dong-Qi Wang [d], Wen-Liang Liu [c,e], Li-Na Xie [a], Shi-Hua Li [a], Li-Shan Tan [a], Bin Zhao [b], Xiu-Zhen Li [a,c], Jian-Wu Tang [a,c]

[a] State Key Laboratory of Estuarine and Coastal Research, Institute of Eco-Chongming, East China Normal University, Shanghai, China
[b] Key Laboratory for Biodiversity Science and Ecological Engineering (Ministry of Education), Fudan University, Shanghai, China
[c] Yangtze Delta Estuarine Wetland Ecosystem Observation and Research Station (Ministry of Education & Shanghai Science and Technology Committee), Shanghai, China
[d] Key Laboratory of Geographic Information Science (Ministry of Education), School of Geographical Sciences, East China Normal University, Shanghai, China
[e] School of Ecological and Environmental Sciences, East China Normal University, Shanghai, China

HIGHLIGHTS

- NEE of the coastal marshes decreased under SLR projection at various scales.
- Decline in NEE was attributed to the unequal responses of GPP and ER to stresses.
- Limited leaf growth and photosynthesis significantly reduced carbon uptake.
- SLR projection reduced plant biomass, soil microbial biomass and enzyme activities.
- Decreased soil nutrients also affected the carbon budget in marsh plants and soil.

GRAPHICAL ABSTRACT

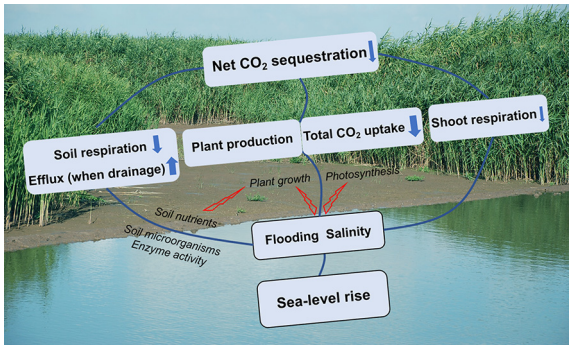

ARTICLE INFO

Article history:
Received 3 April 2020
Received in revised form 22 July 2020
Accepted 22 July 2020
Available online 28 July 2020

Editor: Ashantha Goonetilleke

Keywords:
Coastal wetland
CO_2 fluxes
Sea-level rise
Sensitivity
Plant physiology
Soil biochemistry

ABSTRACT

Coastal marshes have a significant capacity to sequester carbon; however, sea-level rise (SLR) is expected to result in prolonged flooding and saltwater intrusion in coastal regions. To explore the effects of SLR projections on net CO_2 uptake in coastal marshes, we conducted a "double-check" investigation, including the eddy covariance (EC) measurements of the CO_2 fluxes in subtropical coastal marshes along inundation and salinity gradients, in combination with a mesocosm experiment for analyzing CO_2 flux components under waterlogging and increased salinity conditions. During the same measurement periods, the net ecosystem CO_2 exchange (NEE_{EC} based on the EC dataset) in an oligohaline marsh was higher than that in a low-elevation mesohaline marsh, whereas the NEE_{EC} was lower than that in a high-elevation freshwater marsh. The declines in NEE_{EC} between the marshes could be attributed to a greater decrease in gross primary production relative to ecosystem respiration. Waterlogging slightly increased the NEE_{ms} (NEE based on the mesocosms) because of inhibited soil respiration and slight changes in plant photosynthesis and shoot respiration. However, the NEE_{ms} measured during the drainage period decreased significantly due to the stimulated soil respiration. The NEE_{ms} decreased with increasing salinity (except under mild salinity), and waterlogging exacerbated the adverse impacts of salinity. The amplificatory effect of decreases in both leaf photosynthesis and growth under hydrological stresses contributed more to reduce the NEE_{ms} than to respiratory effluxes. Both waterlogging and increased salinity reduced the root biomass, soil microbial biomass, and activities of assayed soil enzymes (except for cellulase under waterlogging conditions), leading to limited soil respiration. The declines in plant growth, photosynthesis, and soil respiration

* Corresponding author at: Estuary & Coast building, 500 Dongchuan Road, 200241 Shanghai, China.
E-mail address: zmge@sklec.ecnu.edu.cn (Z.-M. Ge).
[1] These authors contributed equally

https://doi.org/10.1016/j.scitotenv.2020.141214

could also be attributed to the decrease in soil nutrients under waterlogging and increased salinity conditions. We propose that the coupling of SLR-driven hydrological effects lowers the capacity of CO_2 uptake in subtropical coastal marshes.

1. Introduction

Coastal wetlands, especially tidal marshes, mangroves, and seagrass beds, play an important role in the global carbon cycle because of their significant potential to sequester carbon (Chmura et al., 2003; McLeod et al., 2011; Tan et al., 2020). However, they are highly vulnerable to global changes, particularly to sea-level rise (SLR) (Kirwan and Megonigal, 2013; Schuerch et al., 2018). Rising sea levels in the future would increase the frequency and duration of inundation and saltwater intrusion in coastal areas (Ferguson and Gleeson, 2012; Neubauer et al., 2013; Han et al., 2018), potentially affecting carbon dynamics and plant zonation (Neubauer, 2013; Ge et al., 2015; Wilson et al., 2018a).

Net ecosystem CO_2 exchange (NEE) represents a balance between gross primary production (GPP) and ecosystem respiration (ER) that characterizes the net CO_2 uptake capacity of an ecosystem. Generally, increased inundation results in decreased oxygen concentrations and limited CO_2 diffusion as well as elevated ionic and osmotic stress in plants and soil (Pezeshki, 2001; Neubauer, 2013; Rath and Rousk, 2015; Luo et al., 2019). Also, intensified inundation can reduce photosynthetic enzyme activities, stomatal conductance, and photosynthate transport in plants, resulting in decreased photosynthetic carbon fixation (considered as GPP) and NEE (Forbrich and Giblin, 2015; Han et al., 2015; Zhao et al., 2019). Kathilankal et al. (2008) quantified that tidal inundation caused a mean reduction of 46% in NEE in the coastal marshes, coupled with a 66% reduction in GPP throughout the tidal flooding period, when compared to non-flooded conditions. However, Heinsch et al. (2004) reported that tidal flooding can reduce pore salinity and subsequently enhance GPP in marshes dominated by low salinity-tolerant plants.

In contrast, NEE can increase under flooding/waterlogging conditions by inhibiting ER, which includes plant respiration by aerial tissues (shoot respiration, R_{shoot}) and soil respiration (R_{soil}) by roots, soil microbes, and fauna (Morison et al., 2000; Heinsch et al., 2004;). The decreased availability and diffusion of O_2 under inundation conditions restricts the metabolism of plant and soil microbial communities, limiting aerobic respiration (Gleason and Dunn, 1982; Neubauer, 2013; Han et al., 2015). Moreover, the activities of soil enzymes involved in carbon cycling can also be negatively affected by inundating stress (Pulford and Tabatabai, 1988), thus possibly inhibiting microbial CO_2 respiration.

Many studies have shown that high salinity negatively affects the GPP and ER of coastal marshes, thus leading to a decrease in NEE (Neubauer, 2013; Wilson et al., 2015; Krauss et al., 2016; Wilson et al., 2018a, 2018b). Declining GPP under an enhanced salinity environment can be attributed to decreased plant photosynthesis (Sudhir and Murthy, 2004; Wilson et al., 2015), photosynthetic pigment concentrations (Li et al., 2018a), and stomatal conductance (Pagter et al., 2009). With a rise in salinity, ER also becomes limited, mainly due to the suppressed growth of plants and soil microorganisms (Neubauer et al., 2013; Weston et al., 2014; Hu et al., 2015; Rath and Rousk, 2015; Krauss et al., 2016). However, Morrissey et al. (2014) demonstrated that microbial respiration increased under slight salinity (~2 ppt) because of an increase in the bioavailability of organic substrates and enzyme activity.

Previous studies have widely focused on carbon fluxes in coastal ecosystems, especially on how carbon fluxes respond to *in situ* or simulated inundation or elevated salinity (Weston et al., 2014; Krauss et al., 2016; Knox et al., 2018), whereas a few studies have examined both the independent and joint effects of inundation and salinity (Neubauer, 2013; Wilson et al., 2018a). Wilson et al. (2018a) presented that inundation stress exacerbated the negative effects of salinity on CO_2 flux components in a brackish marsh. However, Neubauer (2013) reported that NEE in a freshwater marsh did not change when both salinity and hydrology were manipulated.

In China, roughly half of the coastal marsh area is covered by the common reed *Phragmites australis*. Particularly, the rate of SLR along the coastline of China is much faster than the global average (see Fig. 1a). To explore the effects of prolonged inundation and saltwater intrusion, due to influences from SLR, on net CO_2 uptake in coastal marshes, we conducted two investigations, including (1) the eddy covariance (EC) measurements of the CO_2 flux in the subtropical *P. australis* marshes with regular tidal cycle in the Yangtze Estuary and (2) a mesocosm experiment on CO_2 flux components under waterlogging and salinity conditions. We measured the NEE_{EC} (based on EC techniques) to test the variability of net CO_2 uptake in *P. australis* marshes subjected to increasing degrees of inundation and saltwater intrusion. To further examine the response of CO_2 flux components to the independent and synergistic projections of SLR, we transplanted the plant-soil monoliths of *P. australis* under waterlogging and increased salinity conditions for scaling the NEE_{ms} (based on a mesocosm), plant carbon uptake (photosynthesis), and R_{shoot} and R_{soil}. At the same time, the plant growth (biomass and leaf area) and soil variables (microbial biomass, extracellular enzyme activity, and nutrients) were measured to understand the mechanisms controlling CO_2 flux changes associated with SLR projections. We hypothesized that prolonged inundation and increased salinity would lead to a decrease in net CO_2 uptake with combined hydrological effects caused by unequal responses of GPP and ER, and the variability of CO_2 fluxes could be attributed to changes in plant growth, physiology, and soil microorganisms and nutrients. This study, conducted at various levels, may improve our understanding of how carbon processes in coastal wetlands would respond to future SLR conditions.

2. Materials and methods

2.1. Eddy flux measurements

2.1.1. Study sites

The study area lies in the coastal wetlands of Chongming Island in the Yangtze Estuary (Fig. 1). Chongming Island has an eastern Asian monsoon climate with an average annual temperature of 15.2–15.8 °C, average annual precipitation of approximately 1022 mm, and average humidity of approximately 80%. Tidal movement in this area is irregular and semidiurnal, with the mean and maximum tide heights ranging from 2.0 to 3.1 m and 4.6 to 6.0 m, respectively (Ge et al., 2015).

Three EC towers were installed from the western to eastern marshes with *P. australis* as the dominant species on Chongming Island (Fig. 1b) by Fudan University and East China Normal University in Shanghai, China (Guo et al., 2009; Ma and Lu, 2011). Table 1 lists the primary characteristics of the geographical, hydrological, vegetative, and edaphic properties at the three EC sites. The M-L site (mesohaline marsh with low elevation) is often occupied by saline water because of strong seawater intrusion from the East China Sea. The salinities of the tidal water and soil surrounding the M-L site can be as high as 10–15 ppt and 2500–3000 mg L^{-1}, respectively, during most of the year. The O-M site (oligohaline marsh with medium elevation) lies in the middle area between fresh runoff and seawater, such that this site has annual average surface water and soil salinities of 3–5 ppt and 1500–2000 mg L^{-1}, respectively. The F-H site (freshwater marsh with high elevation) located near the mainstem of the Yangtze River is

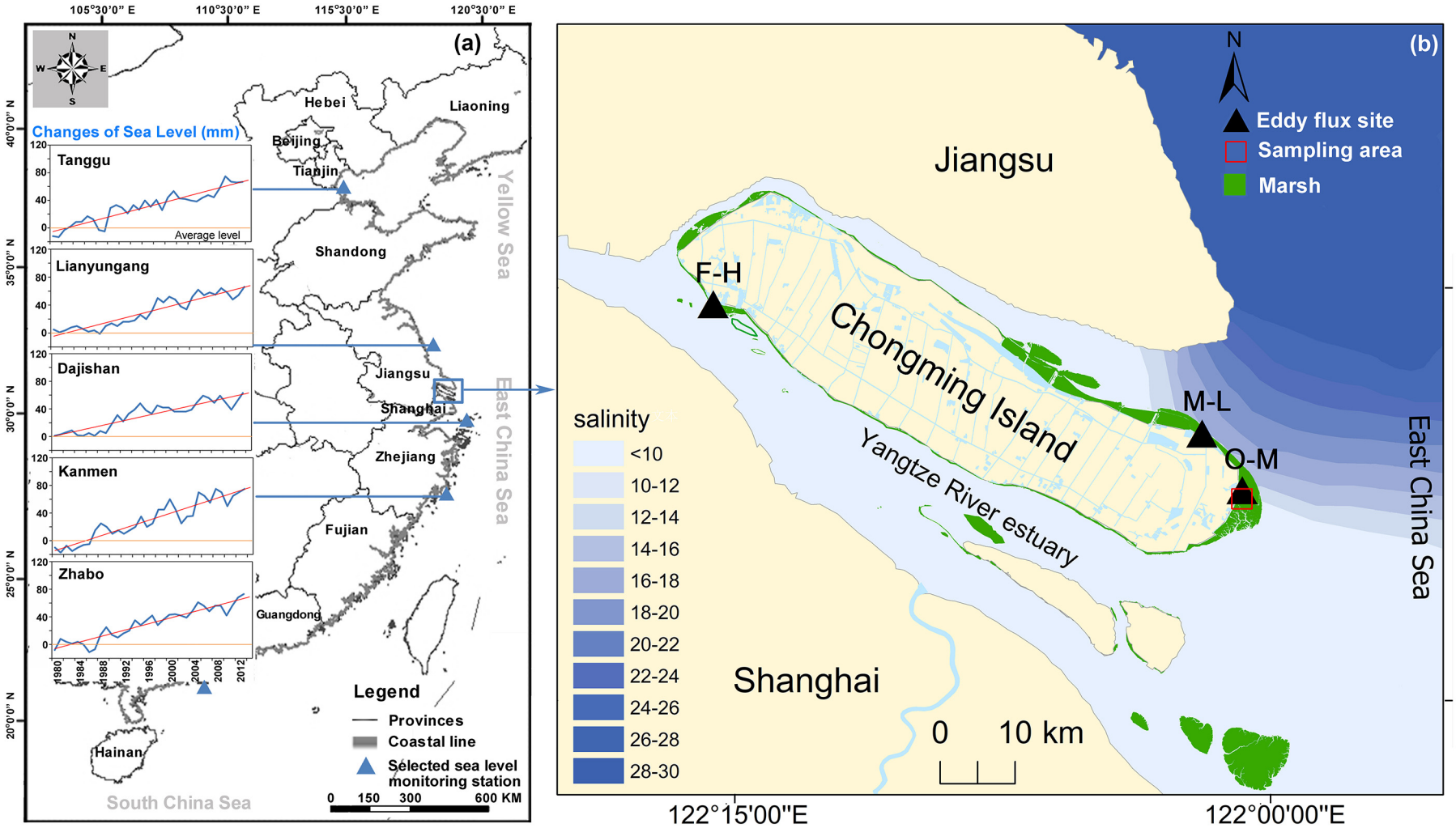

Fig. 1. (a) Historical changes in sea level along China's coastline (State Oceanic Administration, 2018). (b) The location of the eddy covariance (EC) sites in Chongming Island of the Yangtze Estuary. The red frame indicates the sampling location for the plant-soil mesocosm experiment. The data for sea surface water salinity are regularly released by the State Oceanic Administration (China), while the data for surface water salinity during the river flooding season of 2013 are shown (State Oceanic Administration, 2012). (For interpretation of the references to colour in this figure legend, the reader is referred to the web version of this article.)

Table 1
Primary characteristics of the geographical, hydrological, vegetative, and edaphic properties at three eddy covariance (EC) sites.

Site	M-L site	O-M site	F-H site
Marsh type	Mesohaline marsh	Oligohaline marsh	Freshwater marsh
Salinity of surface water (ppt)	10–15	3–5	<0.5
Marsh elevation (m)	~3.3	~3.5	~4.0
Inundation duration (h day^{-1})[a]	~4.5	~3.0	~1.0
Dominant vegetation	*Phragmites australis* *Spartina alterniflora*	*P. australis* *S. alterniflora*	*P. australis*
Aboveground biomass (g m^{-2})	965.6 ± 82.0	1170.0 ± 103.1	2133.1 ± 158.5
Leaf area index (m^2 m^{-2})	3.84	4.70	5.59
Soil salinity (mg L^{-1})	2500–3000	1500–2000	<150
Soil total C (%)	1.70	2.10	2.30
Soil total N (%)	0.08	0.12	0.14
EC flux records	2005–2007 (Jan.–Dec.)	2005–2007 (Jan.–Dec.) 2010–2011 (Jan.–Aug.)	2010–2011 (Jan.–Aug.)

[a] Estimates according to the nearest hydrographical gauging stations, as the Hengsha station for the M-L and O-M sites, and the Nanmen station for the F-H site.

characterized by fresh water runoff, such that this site is insusceptible to seawater intrusion and has surface water and soil salinities of <0.5 ppt and < 150 mg L^{-1}, respectively, during most of the year.

2.1.2. NEE_{EC} measurements

The EC towers monitored the NEE_{EC} of CO_2 by continuously measuring the 3-D wind and virtual temperature with a three-axis sonic anemometer (CSAT-3, Campbell Scientific Inc., Logan, UT, USA) located on a tower ~4.8 m above the ground surface. An open-path infrared gas analyzer (IRGA; Li-7500, Li-Cor Inc., Lincoln, NE, USA) was used to measure CO_2 concentrations at a frequency of 10 Hz. The meteorological parameters were measured using an array of sensors. Net radiation was measured with four-component net radiometers (CNR1, Kipp and Zonen, Delft, Holland). Air temperature (T_a) and relative humidity (*RH*) were measured with shielded sensors (HMP-45C, Vaisala, Helsinki, Finland). Photosynthetically active radiation (*PAR*) was measured using the Li-190SB sensor (Li-Cor Inc., Lincoln, NE, USA). The 30-min averages of the CO_2 flux and micrometeorological parameters were recorded. Table 1 lists the available recording durations of the NEE_{EC} values at the sites, showing the overlapped measurement periods of 2005–2007 for the O-M and M-L sites and 2010–2011 for the O-M and F-H sites. Fig. S1 shows the meteorological variables of T_a, *PAR*, and *RH* during the measurement periods.

Guo et al. (2009) have fully described the quality control of the NEE_{EC} data and gap-filling procedure. The gaps in the daytime NEE_{EC} were calculated using Eq. (1). The filtered nighttime NEE_{EC} data and air temperature were used to fit an Arrhenius equation (Eq. (2) from Lloyd and Taylor (1994)) with a reference temperature (T_r) of 283.16 K. The estimated nighttime NEE_{EC} was used to estimate the daytime ER. The GPP values were calculated from the values of NEE and ER.

$$\mathrm{NEE} = \mathrm{ER} - \frac{e_0 \times \mathrm{PPFD} \times \mathrm{GPP_{max}}}{e_0 \times \mathrm{PPFD} + \mathrm{GPP_{max}}} \quad (1)$$

where e_0 is the apparent quantum yield, PPFD is the photosynthetic photon flux density, and GPP_{max} is the maximum rate of photosynthesis at light saturation.

$$\mathrm{ER} = \mathrm{ER_r} \ \exp\left\{\frac{E_a}{R}\left(\frac{1}{T_r} - \frac{1}{T_a}\right)\right\} \quad (2)$$

$$\mathrm{GPP} = \mathrm{ER} - \mathrm{NEE} \quad (3)$$

where ER_r is the ecosystem respiration at a referred air temperature, E_a is the activation energy, R is the gas constant, and T_a is the air temperature.

2.2. Mesocosm experiments

2.2.1. Plant-soil monoliths sampling and experimental setup

In the winter (December) of 2015, intact (unbroken) soil blocks of the *P. australis* marsh were excavated near the O-M site in the eastern coastal wetland of Chongming Island (see Fig. 1). A total of 48 mesocosms, consisting of soil monoliths (L-W-H: 32 cm × 24 cm × 40 cm, matching the size of polyethylene containers) with *P. australis* rhizomes, were placed in polyethylene containers. Soil material from the same sampling site was collected to fill small gaps in the containers. The plant growth and soil properties at the sampling site were homogeneous, and the *P. australis* seedlings had the same life forms. All mesocosms were grown in a ventilated and transparent greenhouse (seasonal temperature and *RH* shown in Fig. S3). A hose with a valve was installed at the bottom of each container to control drainage and water level.

During the plant dormancy period (January and February) of 2016, all mesocosms were watered daily using freshwater to homogenize soil salinity. Buds appeared at the beginning of March 2016, and the mesocosms were fertilized once with revised Hoagland's nutrient solution. The densities of buds in the growing containers were relatively homogenous before treatments. The single-variable experiments comprised two waterlogging treatments, including a non-waterlogged group (control group, water table at 15–20 cm below the soil surface) and a waterlogged group (the water level was maintained at ~100 mm above the soil surface), and four salinity treatments, including a freshwater-treated group (control group) and three saline water (5, 15, and 30 ppt)-treated groups (using a sodium chloride solution). The treatments for the double-variable treatments (two waterlogging × four salinity conditions) were simultaneously established. Six replicates were setup for each single- and double-variable hydrological treatment. Every two weeks, all mesocosms were drained for 12 h to renew irrigation (also for flux measurements during drainage, see Sections 2.2.2 and 2.2.5). The drainage duration was roughly similar to the local semidiurnal tidal movement in the marsh zones. Freshwater was used to maintain the water level during the non-irrigation period to avoid excess salt accumulation resulting from water evaporation. The incubation experiment of the mesocosms occurred during the period from March to November of 2016–2017.

2.2.2. NEE_{ms} measurements

Static enclosed transparent chambers were used to measure the net CO_2 fluxes of the *P. australis* plant-soil mesocosms (according to Krauss et al., 2016). The sampling chamber (L-W-H: 38 cm × 30 cm × 100 cm) had a top that could be closed and an open bottom that was made from 5-mm thick transparent Perspex. Three electric fans and a rubber tube with a length of 20 cm and an inner diameter of 0.5 cm were mounted on the top of each chamber, where the end of the tube was sealed with a three-way valve. All rubber hoses and joints were sealed with silica gel to ensure air tightness during gas sampling.

Gas samples were collected on clear days in April, June, August, and October of 2016; samples were collected at 9:00 AM, 12:00 PM, 3:00 PM, and 6:00 PM for 30 min each. To avoid leakage of CO_2, the bottom of the chamber was inserted into the U-shaped stainless-steel

groove fixed (by silica gel) at the top of the incubation containers (see Fig. S3) with water seal. During sampling, A 50-mL sample of gas was extracted with a syringe at 0, 10, 20, and 30 min and then injected into the Fluode gas sampling bags. The temperature inside the enclosed chamber was measured using an anemometer (Kestrel-4000, Nielsen-Kellerman Co. Boothwyn, PA, USA). Since tidal activities with inundation and reaeration substantially affect the CO_2 fluxes in costal ecosystems (*e.g.* Guo et al., 2009), we also determined the NEE_{ms} values for all mesocosms during the drainage period (mentioned in 2.2.1 chapter). Gas samples were collected after 12 h of drainage under both non-waterlogging and waterlogging treatments.

The CO_2 concentrations were determined using a gas chromatograph (GC Systems, Santa Clara, CA, USA) equipped with a flame ionization detector (FID). The operating temperature of the detector was set to 200 °C, with nitrogen used as the carrier gas at a flow rate of 30 mL min^{-1}.

The NEE_{ms} values were calculated using the box gas flux formula as follows:

$$NEE_{ms} = \frac{\Delta CO2}{\Delta t}\frac{V}{A} \quad (4)$$

where $\Delta CO_2/\Delta t$ is the change in the concentration of CO_2 over time (t), V is the volume of the enclosure, and A is the cross-sectional area of the enclosure.

We checked for the data quality due to potential leakage or saturation, by implementing a linear regression. The flux values were discarded when the correlation coefficient of the regression lower than $R^2 = 0.85$.

2.2.3. Measurement of photosynthetic rate and leaf area

The net rates of photosynthesis (P_N) and light response curves were measured using a portable photosynthesis system (Li-Cor 6400XT, Li-Cor Inc., Lincoln, NE, USA) on the clear days of April, June, August, and October of 2016 (see Table S1 for details). The fully expanded mid-canopy leaves from three plants in each container were randomly selected for measurement. The measurements were conducted between 8:00 AM and 11:00 AM, at photosynthetic photon flux densities (PPFD) of 0, 20, 40, 60, 80, 100, 200, 400, 600, 800, 1200 and 1600 μmol m^{-2} s^{-1} under a constant saturated CO_2 concentration. The leaf chamber was maintained at a temperature of 25 ± 1 °C, a vapor pressure deficit of 1.0 kPa, and an RH of 60%. Following Thornley (1998), the light response curves were modeled by fitting the P_N data to a non-rectangular hyperbola equation using a nonlinear least squares regression to calculate the light-saturated maximum rate of photosynthesis (P_{max}). The P_{max} was identified as the indicator of photosynthesis capacity in this study. To approximately upscale the leaf-scale photosynthesis to canopy-scale carbon uptake, the number of plants and the total leaf area in each container were measured *in situ*, and thus the maximum rate of photosynthesis at the canopy scale ($P_{max.C}$) was roughly estimated.

$$P_N = \frac{Q_a PPFD + P_{max} - \sqrt{(Q_a PPFD + P_{max})^2 - 4\theta Q_a PPFD P_{max}}}{2\theta} - R_d \quad (5)$$

$$P_{max.C} = P_{max} \times \text{Leaf area} \quad (6)$$

where Q_α is the apparent quantum yield (the initial slope of the light response curve), R_d is dark respiration rate, and θ is a dimensionless fitting parameter.

2.2.4. Measurement of shoot respiration

Li et al. (2018a) had determined the growth parameters (density, shoot height, and aboveground biomass) of *P. australis* under waterlogging and salinity treatments. To assess the CO_2 respiration of aboveground shoots (R_{shoot}), we isolated the shoots from the roots and soil in each mesocosm based on the modified sampling apparatus (according to Kutzbach et al., 2004). In April, June, August, and October of 2016, one medium-sized shoot from each mesocosm was enwrapped in a black polyethylene columnar bag from plant top to bottom. The bottom opening of the bag was tied around the base of the shoot using three soft steel clamps to seal the bag. The sampling port, with a three-way valve, was installed on the polyethylene bag ~50–75 cm above the soil surface. Ambient air was filled into the bags using an air pump. After 30 min, a 50-mL sample of gas was extracted with a syringe and then injected into the Fluode gas sampling bag. Ambient air was also simultaneously collected to determine the background CO_2 concentration.

The CO_2 concentrations in the Fluode gas sampling bags ($[CO_2]_{sample}$) and background values ($[CO_2]_{ambient}$) were determined using a gas chromatograph (GC Systems, Thermo Fisher Scientific Inc., Waltham, MA, USA) equipped with an FID (methodology mentioned above). The R_{shoot} in each mesocosm was estimated as follows:

$$R_{shoot} = \frac{1000\left([CO_2]_{sample} - [CO_2]_{ambient}\right) \times V_{sample}}{3600 \times V_m \times t_{sample}} \quad (7)$$

where V_{sample} is the effective volume of the polyethylene bag, V_m is the molar volume of CO_2 gas at 1 atm of pressure, and t_{sample} is the sampling duration (0.5 h).

2.2.5. Measurements of soil respiration and root biomass

To avoid interference between the measurements of NEE_{ms} and plant photosynthesis/respiration, the R_{soil} rates were measured in April, June, August, and October of 2017 using a R_{soil} chamber (LI-6400-09, Li-Cor, Inc., Lincoln, NE, USA) connected to a portable IRGA. Before measurement, a PVC soil collar, with an inner diameter of 10 cm, was permanently mounted in the middle of each mesocosm. The soil collars were inserted approximately 5 cm into the soil, after which the living plants inside were carefully clipped from the soil surface. The CO_2 concentration at the soil surface was measured (~380–450 μmol mol^{-1}) and set as the target concentration for each measurement cycle. The R_{soil} chamber was vertically inserted into the soil collar for three measurement cycles. Each measurement cycle represented a single and short-duration (~5 min) static flux measurement. Soil temperature near the collar was measured simultaneously using a thermocouple penetration probe (LI-6400-09 TC, Li-Cor, Inc., Lincoln, NE, USA).

Furthermore, we measured the R_{soil} values for all mesocosms after 12 h of drainage (mentioned in Section 2.2.1) under both non-waterlogging and waterlogging treatments.

In October 2017, the root biomass in each mesocosm was assessed using stainless-steel pipes (4.2 cm in diameter) from the soil surface to the container bottom. The soil material was washed away using tap water through a 60-mesh screen. The living roots were picked and dried to a constant weight at 60 °C.

2.2.6. Assay of soil microbial biomass and enzyme activities

In October 2017, steel corers with an inner diameter of 2 cm were used to randomly extract 10 soil cores (15 cm depth) in each container for determining the microbial biomass carbon (MBC) and extracellular enzyme activity. The soil around the roots at ~1 cm was collected and mixed. The soil samples were freeze-dried immediately, sieved to 0.6 mm, and stored at 4 °C. The soil MBC was measured using the chloroform fumigation and direct extraction technique (Vance et al., 1987). Carbon was extracted with 0.5 M K_2SO_4 from both fumigated and nonfumigated samples and measured using an elemental analyzer (Elementar Vario EL III CHNOS, Elementar Analysensysteme GmbH, Langenselbold, Germany), and MBC was estimated using the following formula: MBC = (C from fumigated – C from nonfumigated)/0.38.

The activity of the soil enzymes sucrase and cellulase were assayed to track changes in the carbon source of soil organic matter and to obtain mechanistic insights into the soil carbon loss pathways. According to Frankeberger and Johanson (1983), the sucrase activity was analyzed using 3,5-dinitrosalicylic acid colorimetry and expressed as mg glucose hydrolyzed from sucrase g^{-1} dry sample per 24 h at 37 °C. The cellulase activity was analyzed using 3,5-dinitrosalicylic acid colorimetry and expressed as mg glucose equivalents hydrolyzed from sodium carboxymethyl cellulase g^{-1} dry sample per 72 h at 37 °C. All assays included appropriate blanks in each group.

2.2.7. Measurement of soil properties

In October 2017, the root-free soil was mixed, air-dried and ground into a powder. The soil particles were then sieved by passing through a 1-mm sieve to determine the conventional chemical indicators. Soil organic carbon (SOC) and total nitrogen (TN) were determined using an elemental analyzer (Elementar Vario EL III CHNOS, Elementar Analysensysteme GmbH) after the samples were acidified with 1 mol L^{-1} HCl. The content of alkali-hydrolyzable nitrogen (AN) was determined using the alkaline hydrolysis diffusion method and that of available phosphorus (AP) was determined using the molybdenum blue colorimetric method after extraction with 0.5 mol L^{-1} sodium bicarbonate. The C:N ratio was calculated as the ratio between SOC and TN. The oxidation-reduction potential (ORP) was measured directly using a portable ORP sensor (SX712, Sanxin Co., Shanghai, China).

2.3. Data analyses

In this study, the negative NEE values represented a CO_2 sink from the atmosphere, while the positive values indicated CO_2 emissions to the atmosphere. For the NEE_{EC} values measured in the field, a paired-samples *t*-test was used to compare the daily NEE_{EC} values among different sites during the overlapping measurement periods (O-M site *vs.* M-L site from 2005 to 2007 and O-M site *vs.* F-H site from 2010 to 2011). The data groups of flux components (NEE_{ms}, P_{max}, $P_{max.C}$, R_{shoot}, and R_{soil}) for the mesocosms met the assumptions of normality (Kolmogorov-Smirnov test). A one-way analysis of variance (ANOVA), along with the Tukey's post-hoc test, was used to compare under different waterlogging and salinity conditions. A two-way ANOVA was used to assess the effects of waterlogging, salinity, and their interactions with flux components, plant growth parameters (leaf area and root biomass), and soil microbial variables (MBC, enzyme activities, and nutrients). The level of statistical significance was set to $P < 0.05$. The Spearman's correlation analysis was used to examine the relationships among the CO_2 flux components (NEE_{ms}, $P_{max.C}$, R_{shoot}, and R_{soil}) and plant and soil variables (leaf area, root biomass, MBC, and soil enzyme activities). The statistical analyses were performed with SPSS for Windows 19.0 (SPSS, Inc., Chicago, IL, USA.).

Furthermore, redundancy analyses (RDA) was used to test the effects of hydrological factors (waterlogging and salinity) on carbon flux components, plant growth, and soil variables. A min-max normalization was used to normalize the NEE values for the RDA. The RDA was performed with CANOCO 4.5 (Microcomputer Power, Ithaca, NY, USA).

The relative changes (Δ) in both the NEE_{EC} (also the components of GPP and ER) measured in the field and the NEE_{ms} (also components of $P_{max.C}$, R_{shoot}, and R_{soil}) measured for the plant-soil mesocosms during the growing period (April–October) were determined as follows:

$$\Delta NEE_{EC}(\&components) = \frac{NEE_{EC}(ML) - NEE_{EC}(OM)}{NEE_{EC}(OM)} \times 100\% \& \frac{NEE_{EC}(OM) - NEE_{EC}(FH)}{NEE_{EC}(FH)} \times 100\% \quad (8)$$

$$\Delta NEE_{ms}(\&components) = \frac{NEE_{ms}(treatment) - NEE_{ms}(control)}{NEE_{ms}(control)} \times 100\% \quad (9)$$

where $NEE_{EC}(ML)$, $NEE_{EC}(OM)$, and $NEE_{EC}(FH)$ are the average values of the monthly NEE_{EC} at the M-L, O-M, and F-H sites, respectively, and the $NEE_{ms}(treatment)$ and $NEE_{ms}(control)$ are the values of the flux components under hydrological treatments and the control group, respectively.

3. Results

3.1. NEE_{EC} based on EC data

Throughout the overlapped measurement period (2005–2007) for the O-M and M-L sites, the daily (as well as monthly) NEE_{EC} at the O-M site was 18.0% ($t = -6.686$, $df = 1077$, $P < 0.001$) higher than that at the M-L site (Fig. S2 & Fig. 2). The annual cumulative NEE_{EC} values at the O-M site (−739.4 g C m^{-2} yr^{-1} in 2005 and − 700.2 g C m^{-2} yr^{-1} in 2007) were 35.5% and 21.6% higher than those at the M-L site (−477.2 g C m^{-2} yr^{-1} in 2005 and − 547.2 g C m^{-2} yr^{-1} in 2007) in 2005 and 2007, respectively (Fig. 2). The annual cumulative NEE_{EC} exhibited little difference between these two sites in 2006 (−885.4 g C m^{-2} yr^{-1} at the O-M site and −911.5 g C m^{-2} yr^{-1} at the M-L site).

During the overlapped measurement period (2010−2011) for the O-M and F-H sites, the daily (as well as monthly) NEE_{EC} at the O-M site was 18.3% lower ($t = -3.860$, $df = 481$, $P < 0.001$) than that at the F-H site (Fig. S2 & Fig. 2). The annual cumulative NEE_{EC} values at the O-M site (−299.6 g C m^{-2} yr^{-1} in 2010 and −202.2 g C m^{-2} yr^{-1} in 2011) were 9.1% and 19.9% lower than those at the F-H site (−329.7 g C m^{-2} yr^{-1} in 2010 and −252.4 g C m^{-2} yr^{-1} in 2011) in 2010 and 2011, respectively (Fig. 2).

Within the growing seasons (April–October) from 2005 to 2007, the NEE_{EC} values at the M-L site was 0.9–37.8% lower than that at the O-M site (Fig. 4a). Except for 2006, the decrease rates of GPP (16.5% in 2005 and 16.9% 2007) at the M-L site, compared to the O-M site, were greater than those of ER (0.6% in 2005 and 8.5% in 2007). The NEE_{EC} values at the O-M site were lower by 21.5% and 19.0% relative to the F-H site during the growing seasons of 2010 and 2011, respectively, and the decrease rates of GPP (19.8% in 2010 and 12.9% in 2011) were higher than those of ER (18.6% in 2010 and 10.2% in 2011) (Fig. 4a).

3.2. Carbon fluxes based on mesocosms

3.2.1. NEE_{ms} of plant-soil monoliths

Regardless of the salinity treatments, the NEE_{ms} of the plant-soil mesocosms under waterlogging was 6.8% higher than that under non-waterlogging conditions throughout the measurement period (Fig. 3a & b). However, the NEE_{ms} measured during the drainage period decreased by an average of 55.7% and 65.9% for non-waterlogging and waterlogging treatments, respectively, compared to the measurements before drainage (Fig. S5). Irrespective of the waterlogging treatment, the NEE_{ms} values decreased with salinity by 1.2%, 40.5%, and 58.7% at 5, 15, and 30 ppt, respectively, compared with the control groups (0 ppt) throughout the measurement period. The NEE_{ms} values exhibited a declining trend with increasing salinity, except for the 5 ppt treatment in April and June, and for the 30 ppt treatment in April and August under waterlogging conditions (Fig. 3a & b). The lowest NEE_{ms} was found under the combined treatments of waterlogging and 30 ppt salinity, which was even characterized by a positive value, reflecting net CO_2 emissions under waterlogging conditions.

The ANOVA test indicated that waterlogging had a nonsignificant effect on the NEE_{ms}, whereas salinity had a significant ($P < 0.05$) effect throughout the measurement period (Table S2). The influence of waterlogging × salinity on the NEE_{ms} was notable ($P < 0.05$) in April and October.

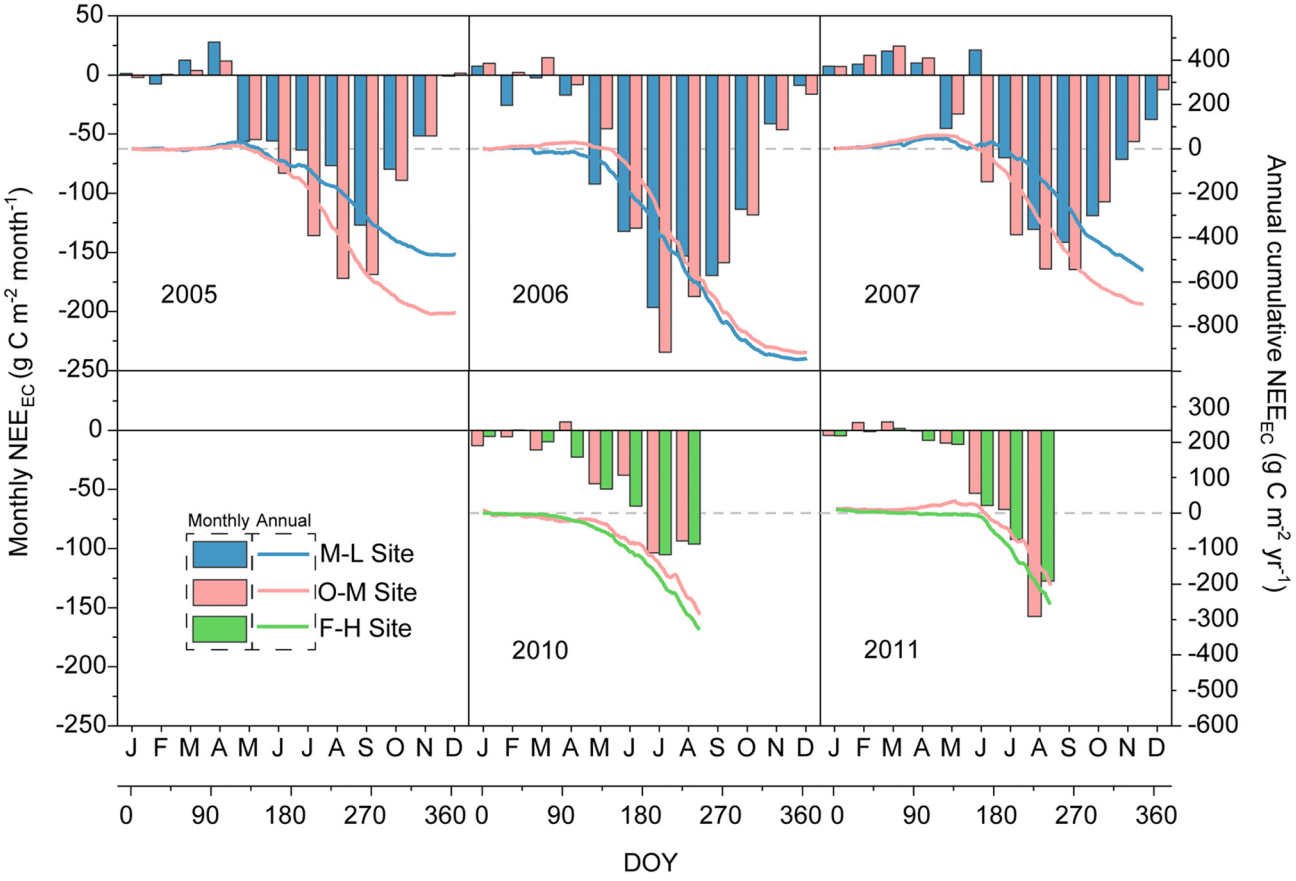

Fig. 2. Monthly and annual cumulative net ecosystem exchange based on eddy covariance dataset (NEE_{EC}) from 2005 to 2007 at the M-L (mesohaline marsh with low elevation) and O-M (oligohaline marsh with medium elevation) sites and from 2010 to 2011 at the O-M and F-H (freshwater marsh with high elevation) sites.

3.2.2. Plant carbon uptake

Regardless of the salinity treatments, the P_{max} at the leaf scale and $P_{max.C}$ at the canopy scale under waterlogging conditions were, on average, 11.6% and 20.3% lower than those under non-waterlogging conditions, respectively, over the measurement period (Fig. 3c–f). Irrespective of the waterlogging treatments, the P_{max} values in the 5, 15, and 30 ppt treatments were, on average, 11.4–55.8% lower than those of the control group over the measurement period. Owing to a significant decrease in leaf area (see Fig. S4), $P_{max.C}$ was more heavily suppressed by salinity and decreased, on average, by 23.4–82.9% with increasing salinity, relative to the control groups (Fig. 3e & f). In general, the P_{max} and $P_{max.C}$ values of *P. australis* exhibited a declining trend with a rise in salinity, where the lowest values were observed under the combined treatments of waterlogging and 30 ppt salinity.

The effect of waterlogging on P_{max} was nonsignificant throughout the measurement period, whereas the effect on $P_{max.C}$ was significant ($P < 0.05$) in June and August (Table S2). Salinity had a significant ($P < 0.05$) effect on the P_{max} values in August and October and on $P_{max.C}$ throughout the measurement period. No significant interactive effect due to waterlogging × salinity was detected for both P_{max} and $P_{max.C}$.

3.2.3. Shoot respiration

The R_{shoot} at non-waterlogging conditions was, on average, 3.9% higher than that under waterlogging conditions, regardless of the saline treatment over the measurement period (Fig. 3g & h). Irrespective of the waterlogging treatments, R_{shoot} decreased, on average, by 3.8%, 20.7%, and 32.6% at 5, 15, and 30 ppt, respectively, compared to the control groups throughout the measurement period (Fig. 3g & h). The lowest R_{shoot} were observed under the combined treatments of waterlogging and 30 ppt salinity in each month.

Waterlogging did not significantly affect R_{shoot}, whereas salinity had a significant ($P < 0.05$) effect over the measurement period (Table S2). Notable ($P < 0.05$) influences of waterlogging × salinity on R_{shoot} were observed in August, June, and October.

3.2.4. Soil respiration, root and soil microbial biomass, and enzyme activities

The R_{soil} value under non-waterlogging conditions was significantly lower (by on average 78.9%, $P < 0.05$) than that under non-waterlogging conditions throughout the measurement period, regardless of salinity treatments (Fig. 3i & j). However, the R_{soil} value measured during the drainage period increased by an average of 2.1 and 19.7 times for non-waterlogging and waterlogging treatments, respectively, compared to the measurements before drainage (Fig. S5). Irrespective of the waterlogging treatments, the R_{soil} values at 5, 15, and 30 ppt decreased, on average, by 9.1%, 17.5%, and 56.4%, respectively, compared to the control groups throughout the measurement period (Fig. 3i & j). In general, the R_{soil} value decreased with increasing salinity, except at 15 ppt under non-waterlogging conditions, as well as at 5 and 15 ppt under waterlogging, in April. The lowest R_{soil} was found under combined treatments of waterlogging and high salinity (15 and 30 ppt). The effects that both waterlogging and salinity treatments had on R_{soil} were significant ($P < 0.05$) over the observation period (except in April) (Table S2). The interactive influence that waterlogging × salinity had on R_{soil} was notable ($P < 0.05$) in June and August.

Irrespective of the salinity treatments, waterlogging decreased the root biomass by an average of 6.1%, MBC by 28.4%, and sucrase activities by 36.0%, relative to non-waterlogging conditions (Fig. 5), whereas the

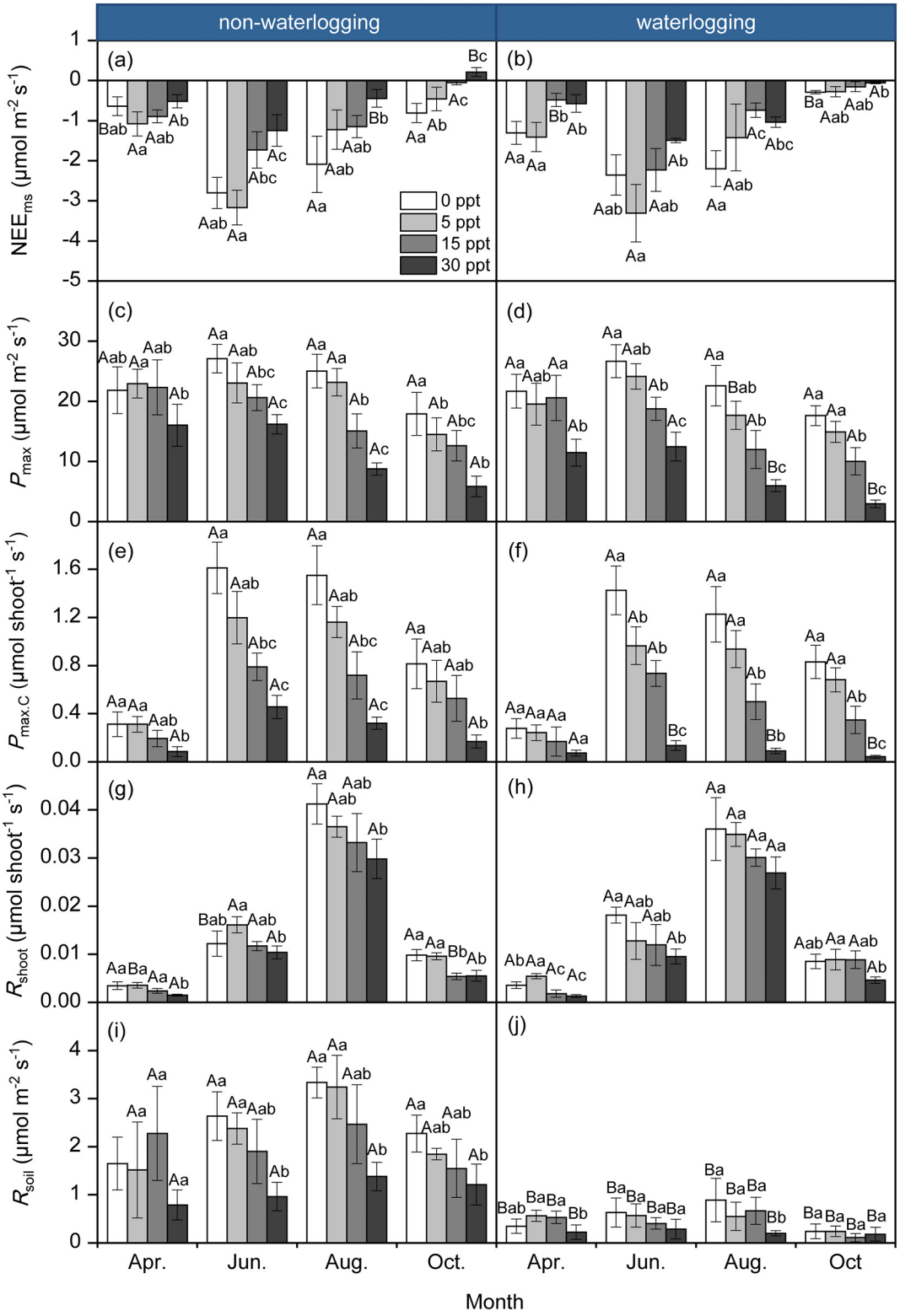

Fig. 3. Seasonal variations in the net ecosystem exchange based on a mesocosm (NEE_{ms}), maximum photosynthesis rate (P_{max}), maximum photosynthesis rate at the canopy scale ($P_{max.C}$), shoot respiration (R_{shoot}), and soil respiration (R_{soil}) of *Phragmites australis* under different waterlogging and salinity treatments. Different capital letters indicate significant differences ($P < 0.05$) between non-waterlogging and waterlogging treatments at the same salinity levels, and different lowercase letters indicate significant differences ($P < 0.05$) among salinity treatments at the same water levels. Fig. S5 presents the changes in NEE_{ms} and R_{soil} measured during the drainage period. Note: the changes in plant photosynthesis and respiration during drainage were negligible.

cellulase activity increased by an average of 62.9%. Regardless of the waterlogging treatments, the root biomass, soil MBC, and cellulase and sucrase activities were lower under high salinity conditions (15 and 30 ppt) than those under freshwater (0 ppt) and mild salinity (5 ppt) conditions (Fig. 5). The lowest root biomass, soil MBC, and assayed enzyme activities were observed under the combined treatments of

waterlogging and high salinity (30 or 15 ppt). Salinity treatments significantly ($P < 0.05$) affected the root biomass. The single and interactive effects of hydrological treatments (waterlogging and salinity) on the MBC and cellulase and sucrase activities in the soil were significant ($P < 0.05$, Table S3).

3.2.5. Degree of changes in NEE_{ms} and its components

Within the growing season (April–October), the rates of change in the NEE_{ms} values of the plant-soil mesocosms under mild salinity (5 ppt) were negligible (0.7 ± 40.3%) compared to the non-salinity groups, regardless of the waterlogging treatments (Fig. 4b & c). The rates of decline in the NEE_{ms} values at 15 and 30 ppt salinities sharply increased relative to the freshwater groups, which showed a greater declining rate (on average 52.2 ± 50.1%) under waterlogging conditions relative to the non-waterlogging conditions (on average 51.1 ± 22.8%). With increasing salinity, the rates of decline in $P_{max.C}$ increased by, on average, 45.8 ± 26.3% and 53.6 ± 29.5% under non-waterlogging and waterlogging conditions, respectively, compared to the control groups (Fig. 4b & c) and were the highest, followed by the corresponding rates of decline in R_{soil} (25.7 ± 28.4% and 19.9 ± 41.8%) and R_{shoot} (18.5 ± 24.3% and 21.0 ± 31.9%).

3.2.6. Effects of waterlogging and salinity

The results of the RDA analysis showed that waterlogging did not have a strong effect on the NEE_{ms}, $P_{max.C}$, and R_{shoot} (Fig. 6a). Waterlogging heavily inhibited R_{soil}, but positively affected it during the drainage period. All flux components had significant negative correlations with salinity, except for R_{shoot} (Table 2). The NEE_{ms} values had a significant ($P < 0.05$) correlation with plant photosynthesis ($P_{max.C}$ and P_{max}) and leaf area. Both $P_{max.C}$ and R_{shoot} had significant ($P < 0.05$) positive correlations with leaf area (Table 2), and R_{soil} had significant ($P < 0.05$) correlations with the root biomass, soil MBC, and sucrase activity under non-waterlogging conditions. During the drainage period, R_{soil} had significant ($P < 0.05$) correlations with the sucrase and cellulase activities under waterlogging treatments.

As shown in Fig. 6b, waterlogging negatively affected the assayed plant and soil variables, except for a positive relationship with cellulase activity. The plant growth (leaf area and root biomass) and soil microbial variables were significantly ($P < 0.05$) negatively affected by salinity, except for the cellulase activity (Table 2).

4. Discussion

4.1. Effects of prolonged flooding

Although the variances in tidal inundation duration and water salinity were coupled at the EC sites, there might be a negative influence of increased inundation on the NEE. Based on the mesocosm experiment, we found that the photosynthetic rate of *P. australis* decreased by 11.6 ± 5.6% under waterlogging compared to non-waterlogging conditions. The waterlogging treatment did not significantly affect the shoot height and aboveground biomass (data not shown) of *P. australis*, but decreased the leaf growth (leaf area) by 13.4 ± 5.9% relative to the non-waterlogging conditions (Fig. S4), leading to reductions in $P_{max.C}$ from the middle of the growing season. This suggests that the amplificatory effect of waterlogging on both photosynthetic rate and leaf growth leads to a substantial decrease in canopy- or community-scale carbon uptake by plants. As summarized in Table S4,

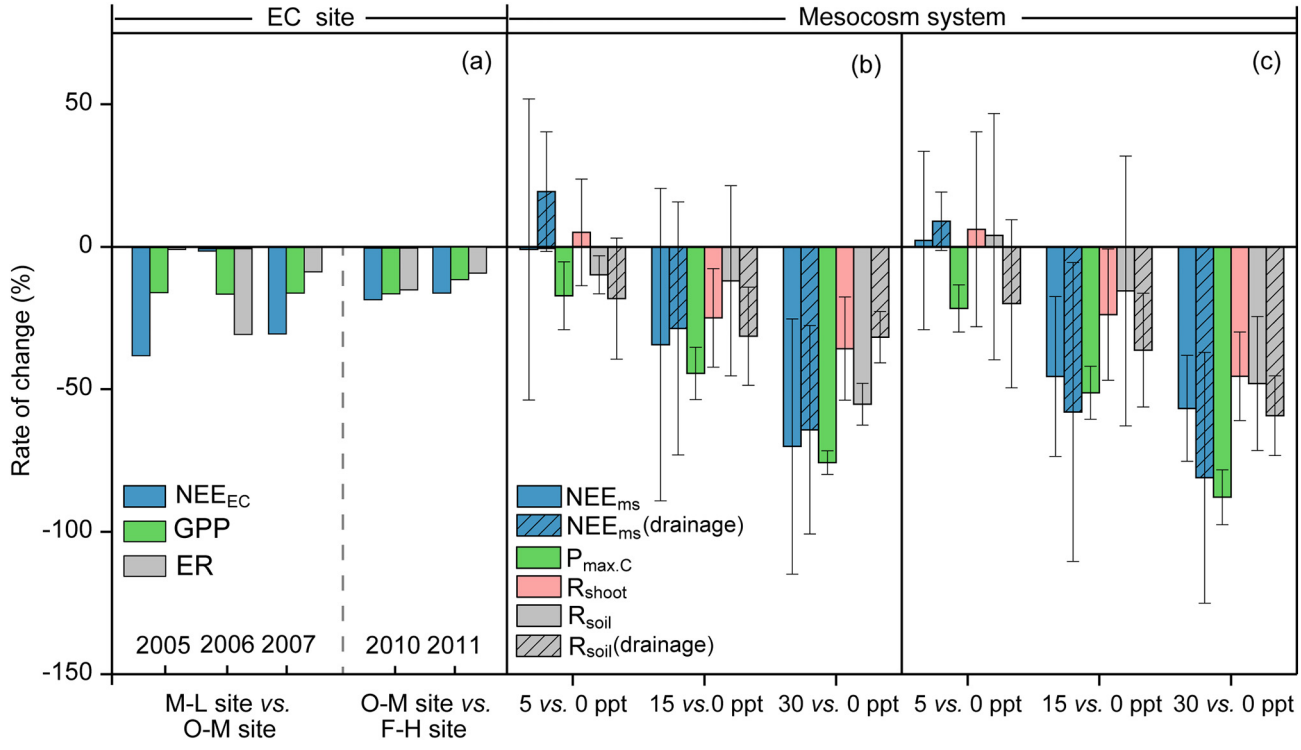

Fig. 4. (a) Rate of change in the net ecosystem exchange based on eddy covariance dataset (NEE_{EC}) [with components of gross primary production (GPP) and ecosystem respiration (ER)] by eddy covariance (EC) measurement sites and NEE based on a mesocosm (NEE_{ms}) [with components of maximum photosynthesis rate at the canopy scale ($P_{max.C}$), shoot respiration (R_{shoot}), and soil respiration (R_{soil})] based on the mesocosm with increasing saline treatments under (b) non-waterlogging and (c) waterlogging conditions during the growing season (April–October). 'M-L (mesohaline marsh with low elevation) site *vs.* O-M (oligohaline marsh with high elevation) site' indicates the rate of change in the NEE_{EC} at the M-L site relative to the O-M site from 2005 to 2007; 'O-M site *vs.* F-H (freshwater marsh with high elevation) site' indicates the rate of change in the average monthly NEE_{EC} at the O-M site relative to the F-H site from 2010 to 2011. '5 *vs.* 0 ppt', '15 *vs.* 0 ppt', and '30 *vs.* 0 ppt' indicate the rates of change in the CO_2 flux components under salinities treatments of 5, 15, and 30 ppt, respectively, relative to the 0 ppt groups. Bars indicate the seasonal deviation.

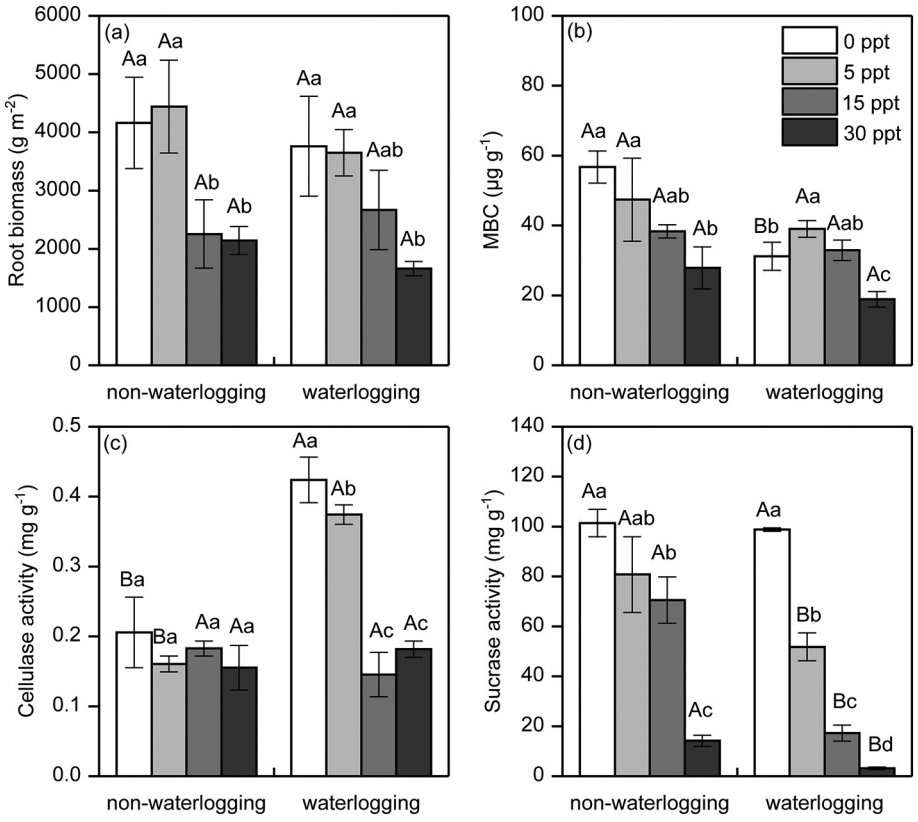

Fig. 5. (a) Root biomass, (b) soil microbial biomass carbon (MBC), (c) sucrase activity, and (d) cellulase activity of *Phragmites australis* soil under different waterlogging and salinity treatments. Different capital letters indicate significant differences ($P < 0.05$) between non-waterlogging and waterlogging treatments at the same salinity levels, and different lowercase letters indicate significant differences ($P < 0.05$) among salinity treatments at the same water levels.

many studies have shown that increased tidal inundation decreased GPP mainly due to reduced photosynthesis in marsh plants, based on various measurement techniques, with a wide range of results (9–82%) (Neubauer, 2013; Forbrich and Giblin, 2015; Wilson et al., 2018a), thus decreasing the NEE (Kathilankal et al., 2008; Han et al., 2015; Zhao et al., 2019). However, Jones et al. (2018) observed that a mild flooding depth (< 10 cm) increased the GPP of a *Spartina alterniflora* marsh because of its strong inundation-tolerance. Therefore, more studies are needed to develop a complete understanding of the relationships between species-specific carbon uptake and intensity of tide inundation.

We found that the NEE_{ms} values under waterlogging conditions were slightly higher than that under non-waterlogging conditions due to a greater reduction in R_{soil} (a major component of CO_2 emission) rather than a decrease in carbon uptake by plants. In addition, root and soil microbial biomass had a positive correlation with R_{soil}, such

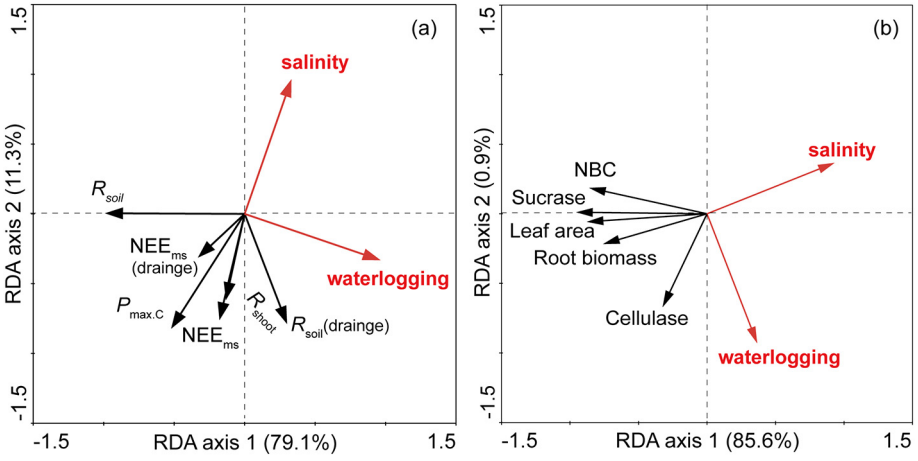

Fig. 6. (a) Ordination diagram based on the redundancy analysis (RDA) of the CO_2 flux components (June as an example) and (b) plant and soil variables with respect to the waterlogging and salinity treatments (red arrows). Note: A vector angle between treatments and variables of less than 90° indicates a positive correlation, whereas an angle more than 90° indicates a negative correlation. Perpendicular vectors (~90°) indicate weak correlation between treatments and variables. (For interpretation of the references to colour in this figure legend, the reader is referred to the web version of this article.)

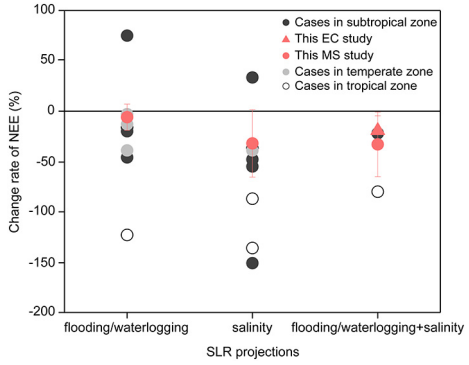

Fig. 7. Global site-specific rates of change in net CO_2 uptake (net ecosystem exchange) in coastal marshes of the subtropical, temperate, and tropical zones (Data see Table S4). EC and MS mean the eddy covariance measurement and mesocosm experiments in this study, respectively.

that a reduction in root biomass and soil MBC (by 9.6 ± 4.4% and 28.0 ± 3.7%, respectively) probably induced a decline in R_{soil}. Previous studies showed that the reduction in ER contributes more to the increase in NEE than the change in GPP when subjected to increased tidal inundation (Heinsch et al., 2004; Neubauer, 2013; Knox et al., 2018; Wilson et al., 2018b). A reduction in CO_2 diffusion rate with inundation directly inhibited soil carbon efflux by the microbial and root aerobic respiration (Heinsch et al., 2004; Davy et al., 2011; Knox et al., 2018). Pezeshki (2001) found that the anoxic roots of marsh plants under waterlogging conditions produced substantial amounts of ethanol or other phytotoxins, thus inhibiting the root biomass and soil MBC.

However, as measured during the drainage period (such as marsh re-exposure during ebb), the R_{soil} under waterlogging treatments increased sharply by approximately 20-fold relative to constant waterlogging, resulting in a significantly decreased NEE_{ms} (Fig. S5). This agrees with the findings of Krauss et al. (2012), who reported a 9-fold increase in R_{soil} when the inundated mesocosms were exposed to air because of the impulsive emission of CO_2 previously produced by roots and microorganisms. In coastal marshes, hot moments of carbon emissions often occur during ebbing after tidal inundation (Li et al., 2018b). Therefore, the stimulated carbon efflux of the exposed marsh after prolonged flooding plays a vital role in the carbon budget.

The R_{shoot} of *P. australis* was not notably affected by shallow flooding treatments. Gleason and Dunn (1982) reported that heavy inundation negatively affects R_{shoot} because of internal hypoxia. The well-developed aerenchyma of *P. australis* allows for its adaptation to shallow waterlogging conditions. In addition, a part of CO_2 from R_{soil}, which is transported longitudinally from the roots to the shoots *via* the aerenchyma (Colmer and Greenway, 2005), is then added to the amount of R_{shoot}.

Table 2
Correlation coefficients among the CO_2 flux components, salinity levels, and plant and soil variables (with a salinity gradient) under the non-waterlogging and waterlogging conditions.

Parameters		Independent variables	non-waterlogging	waterlogging
NEE_{ms}	*vs.*	Salinity	−0.43**	−0.34*
P_{max}			−0.65**	−0.75**
$P_{max.C}$			−0.61**	−0.77**
R_{shoot}			−0.20 ns	−0.225 ns
R_{soil}			−0.61**	−0.39**
Leaf area			−0.52**	−0.62**
Root biomass			−0.76**	−0.75**
MBC			−0.89**	−0.52 ns
Sucrase activity			−0.91**	−0.97**
Cellulase activity			−0.25 ns	−0.82**
NEE_{ms}	*vs.*	P_{max}	0.61**	0.55**
	vs.	$P_{max.C}$	0.62**	0.46**
	vs.	Leaf area	0.48**	0.20 ns
$P_{max.C}$	*vs.*	Leaf area	0.94**	0.88**
R_{shoot}	*vs.*	Leaf area	0.79**	0.72**
R_{soil}	*vs.*	Root biomass	0.60**	0.23 ns
	vs.	MBC	0.83**	0.22 ns
	vs.	Sucrase activity	0.91**	0.23 ns
	vs.	Cellulase activity	0.34 ns	0.40 ns
R_{soil} (drainage)	*vs.*	Root biomass	0.23 ns	0.59 ns
	vs.	MBC	0.36 ns	0.19 ns
	vs.	Sucrase activity	0.53 ns	0.78**
	vs.	Cellulase activity	0.39 ns	0.63*

ns = nonsignificant ($P > 0.5$); NEE_{ms}, net ecosystem exchange based on a mesocosm; P_{max}, maximum photosynthesis rate; $P_{max.C}$, maximum photosynthesis rate at the canopy scale; R_{shoot}, shoot respiration; R_{soil}, soil respiration.
* Significance at $P < 0.05$.
** Significance at $P < 0.01$.

4.2. Effects of saltwater addition

Both the EC flux observations and mesocosm experiment exhibited a decline in NEE along an increasing salinity gradient. This can be attributed to the unequal responses of GPP and ER to salinity, showing a larger reduction in GPP (and plant photosynthesis) than in ER (and respiration components) (see Fig. 4). Krauss et al. (2016) and Wilson et al. (2018b) reported similar results. Neubauer (2013) reported that elevated salinity reduced the annual GPP and NEE estimates, due to declining plant growth. Weston et al. (2014) and Wilson et al. (2015) observed that seasonal saltwater can inhibit NEE by depressing plant productivity and reducing organic matter decomposition in coastal marshes.

Based on the mesocosm experiments, both the photosynthesis of *P. australis* and respiration components of plant-soil system decreased when subjected to increased salinity. The effect of mild salinity (5 ppt) on NEE_{ms} is nonsignificant, likely because of the counterbalance between the similar degree of reduction in carbon uptake and emission. Under high salinity, we observed a decline in NEE_{ms} based on a larger change in gross carbon uptake (higher sensitivity in $P_{max.C}$) compared with respiration components, resulting from the up-scaling decline in photosynthetic rate and leaf area. Our previous study showed that high salinity reduced the concentration of photosynthetic pigments and aboveground biomass of *P. australis* (Li et al., 2018a), likely contributing to a decrease in NEE_{ms}. Increased osmotic pressure and decreased K^+:Na^+ and K^+:Cl^- ratios under saline conditions, as well as limited stomatal conductance, resulted in reduced photosynthetic capacity (Sudhir and Murthy, 2004; Pagter et al., 2009). A decline in plant growth can be also due to a decrease in soil nutrients with increasing salinity (Fig. S6), because high salinity can suppress microbial growth and nitrogen mineralization in soil and reduce plant productivity and litter input, leading to a decrease in available N and P (Laura, 1977; Hadas et al., 2004).

In this study, the root biomass, MBC, and sucrase and cellulase activities in *P. australis* soil were suppressed by increased salinity, indicating a positive relationship with R_{soil}. Suppressed root respiration of marsh plants can be partially attributed to decreased root productivity and metabolic rates (Krauss et al., 2012). Under a saline environment, external ion concentrations in soils produce high osmotic pressure in microbes, interfering with cellular functions and microbe reproduction (Ikenaga et al., 2010). Therefore, increased osmotic stress under high salinity decreases the microbial biomass or causes cell lysis, thus suppressing microbial respiration (Rath and Rousk, 2015). Moreover, elevated salinity can directly suppress extracellular enzyme activities by affecting molecular stability and protein confirmation states, leading to reduced rates of soil CO_2 production (Tripathi et al., 2007; Neubauer et al., 2013). Based on our experiment, the effects of mild salinity (5 ppt) on the root and soil microbial biomass and R_{soil} were unremarkable. This could be attributed to the adaptation of soil microorganisms from a brackish marsh under mild saline environment (*e.g.*, Morrissey et al., 2014; Wilson et al., 2018a).

The R_{shoot} of *P. australis* roughly did not change at 5 ppt salinity relative to the 0 ppt group, which may be due to steady leaf respiration. Under high salinity conditions (15 and 30 ppt), a significant decrease was observed in R_{shoot}. Schwarz and Gale (1981) reported that an apparent toxic effect induced a decline in maintenance respiration in salt-tolerant plants under high salinity. Suppressed R_{shoot} under high salinity can also be due to limited electron consumption and less CO_2 production in plants (Koyro, 2006).

4.3. Effects of coupling SLR projections

In coastal ecosystems, SLR projections may lead to a positive feedback between prolonged saltwater inundation and increased soil salinity and hypoxia (Ferguson and Gleeson, 2012; Neubauer et al., 2013; Han et al., 2018). The independent effects that inundation and salinity have on the carbon fluxes in coastal marshes have been widely studied, whereas only a few studies have examined the joint effects (*e.g.*, Table S4). Based on our flux monitoring at the marshes, the NEE_{EC} values decreased along an increasing tidal level and salinity gradients. Decreased plant growth (see aboveground biomass and leaf area in Table 1) with an increase in inundation and salinity might explain the reduction in GPP. Furthermore, our mesocosm experiments showed that NEE_{ms} decreased significantly under the combined treatments of waterlogging and increased salinity (except at 5 ppt), relative to non-waterlogged and non-salinity conditions. The negative effects of high salinity (15 and 30 ppt) on NEE_{ms}, $P_{max.C}$, and R_{soil} were exacerbated when coupled with waterlogging, as indicated by the lowest values of these parameters under the combined waterlogging and 30 ppt salinity conditions. Compared with the single-salinity effects, a decrease in the amplitudes of the dominant CO_2 flux components under combined stresses increased both $P_{max.C}$ (from 51.5 ± 7.1% to 62.4 ± 8.1%), and R_{soil} (from 28.0 ± 15.7% to 84.9 ± 7.8%). Wilson et al. (2018a) reported that inundation exacerbated the effects of salinity (from 10 to 20 ppt) on all CO_2 flux components in coastal marshes, *i.e.*, 80.6% *vs*. 86.9% for NEE, 63.4% *vs*. 72.5% for GPP, and 41.6% *vs*. 88.6% for ER under single-salinity and combined conditions, respectively.

The growth and carbon uptake of *P. australis* were highly sensitive to combined waterlogging and increased salinity. Lund et al. (2010) analyzed the data on CO_2 exchange obtained from 12 wetland sites across Europe and North America and concluded that leaf area has a significant correlation with GPP. Therefore, a sharp decline in $P_{max.C}$ under combined treatments of waterlogging and salinity can be mainly attributed to a decrease in leaf area and photosynthetic performance. Waterlogging can interact with salinity to increase the concentrations of salt ions in plant organs, thus restricting plant growth or survival (Barrett-Lennard, 2003). Our statistical results show that the interactive effects of waterlogging and salinity on the photosynthetic rate were not significant likely because of the shallow flooding depth. Nevertheless, both R_{soil} and R_{shoot} were notably affected by the interaction between waterlogging and salinity. In addition to hypoxia and salt ion toxicity stress, the SOC, TN, AN, and AP in soil were the lowest under the combined treatments of waterlogging and high salinity (Fig. S6). Spalding and Hester (2007) demonstrated that the environmental stresses inhibit the organic matter availability for soil microorganisms, such that a decrease in root exudates and secretions reduces the availability of nutrients in the soil. The decrease in soil nutrients under combined treatments may also be a probable reason for reduced root growth and soil microbial biomass and consequent R_{soil}.

4.4. Implications for manipulative experiments and future modeling

With the original plant-soil materials, our experiment took the expected flooding prolongation and local salinity range (0–30 ppt) into account, and a shallow inundation depth was set up to avoid a "heavy hammer" simulation of SLR conditions. However, there remain some uncertainties to consider when applying the laboratory results to field sites, because there are challenges associated with mimicking the realistic day-to-day tidal regime (height and range of tide) and seasonal variation of salinity. Compared to the regular inundation and re-aeration cycle in the field, a constant water table employed in our experiment led to moisture saturation and decreased amplitude of soil temperature, therefore which could result in uncertain effects on soil CO_2 processes. Halupa and Howes (1995) presented that slight changes in tidal fluctuation may have crucial influences for soil organic matter cycling in coastal marshes by affecting the water content and decomposition rate of litters. The persistent waterlogging treatment (2 weeks) resulted in a short-term eruption of R_{soil} when drainage, while decreased oxygen availability and redox conditions will limit the aerobic decomposition and carbon mineralization in a long run (Colmer and Greenway, 2005; Neubauer, 2013; Wilson et al., 2018a). On the other hand, the stochastic ebullition of CO_2 gas might also lead to uncertainties in the estimates of NEE and R_{soil} because the release of gas bubble is both spatially heterogeneous and episodic under constant inundation. Although a constant waterlogging treatment may also not reflect the *in-situ* responses of plant photosynthesis and growth (*e.g.*, leaves and roots) to natural tidal inundation, our results to a certain extent are consistent with the previous field observations, showing that the growth of coastal plants was sensitive to the changes in elevation and flooding duration (Pennings and Callaway, 1992; Kathilankal et al., 2008; Kirwan and Guntenspergen, 2012). Future research needs to address more experiments that include intermittent flooding with different duration and frequency, to improve our understanding of coastal carbon processes in interaction with accelerated SLR and concomitant changes in flooding frequency.

Furthermore, coastal ecosystems have unique sedimentary characteristics that typically result in vegetation-tide-sediment interactions (Ge et al., 2019). Tidal wetlands can, to a certain extent, keep pace with SLR *via* sediment recharge and the consequent vertical sediment accretion (Wang et al., 2019). Together with the projections of prolonged flooding and salinity increase, further experimental designs require high frequency inundations and re-exposure, salination and desalination, and sediment input. Flumes with hydraulic recirculation instruments may be an ideal experimental subsystem (*e.g.*, Möller et al., 2014) to determine the coupling interactive effects of both flooding and salinity on the carbon dynamics of coastal ecosystems.

Besides our study in the subtropical marshes, the cases reported in the temperate and tropical marshes showed that the rates of CO_2 uptake were generally reduced to varying degrees under SLR projections (Fig. 7). For another important greenhouse gas, *i.e.*, CH_4, our latest study revealed that its emission at high water level was 2.6-fold greater than that at low water level, and salinity levels of 5 and 15 ppt stimulated CH_4 emissions in *P. australis* marshes (Liu et al., 2019). As a result, the capacity of CO_2 uptake in coastal marshes might become weaker under SLR conditions. This study could potentially help to improve the biogeochemical models of wetlands. For instance, the Wetland-DNDC model can accurately simulate carbon and nitrogen fluxes in different types of wetlands (Zhang et al., 2002), and the Coastal Wetland GHG Model (CWGM) can empirically predict greenhouse gas fluxes in coastal marshes (Abdul-Aziz et al., 2018). Embedded mechanistic responses of carbon processes in plant and soil compartments, in terms of plant photosynthesis, autotrophic respiration, plant growth, and soil effluxes and microbe-driven carbon turnover, to increased flooding and salinity conditions may promote the application of biogeochemical models on the prediction of SLR impacts on the coastal carbon budget.

5. Conclusions

The effects of SLR on net CO_2 uptake in coastal ecosystems require global attention. Our "double-check" investigation based on EC flux observations and component analysis revealed that the net CO_2 uptake of coastal *P. australis* marshes decreased under projected increases in inundation and salinity. During the same measurement periods, the

NEE_{EC} in the oligohaline marsh was higher than that in the low-elevation mesohaline marsh and lower than that in the high-elevation fresh marsh. The decline in NEE_{EC} between the marshes could be attributed to a greater decrease in GPP relative to ER. Under waterlogging treatment for the plant-soil mesocosms, the NEE_{ms} slightly increased due to inhibited R_{soil} and relatively small changes in plant carbon uptake and R_{shoot}. The measurement recorded during the drainage period of the waterlogging treatment, however, exhibited the stimulation of R_{soil}, resulting in a notable decrease in NEE_{ms}. The saline treatment (except mild salinity) played a great role in affecting NEE_{ms}, and waterlogging exacerbated the adverse impacts of salinity. The reduction in both photosynthetic performance and leaf growth under high salinity conditions contributed more to the reduction in NEE_{ms} than the reduction of respiration effluxes. Both waterlogging and increased salinity reduced the root biomass, soil microbial biomass, and activities of assayed soil enzymes (except cellulase under waterlogging conditions), leading to limited R_{soil}. The declines in plant growth, photosynthesis, and R_{soil} could be also attributed to the decrease in soil nutrients under waterlogging and increased salinity conditions. We suggest that the coupling of SLR-induced hydrological effects lowers the capacity of CO_2 uptake in subtropical coastal marshes.

CRediT authorship contribution statement

Ya-Lei Li: Conceptualization, Methodology, Investigation, Formal analysis, Writing - review & editing. **Hai-Qiang Guo:** Conceptualization, Methodology, Investigation, Formal analysis, Writing - review & editing. **Zhen-Ming Ge:** Conceptualization, Methodology, Investigation, Formal analysis, Writing - review & editing. **Dong-Qi Wang:** Conceptualization, Methodology, Investigation. **Wen-Liang Liu:** Investigation. **Li-Na Xie:** Investigation, Formal analysis. **Shi-Hua Li:** Investigation, Formal analysis. **Li-Shan Tan:** Investigation, Formal analysis. **Bin Zhao:** Writing - review & editing. **Xiu-Zhen Li:** Writing - review & editing. **Jian-Wu Tang:** Writing - review & editing.

Declaration of competing interest

The authors declare that they have no known competing financial interests or personal relationships that could have appeared to influence the work reported in this paper.

Acknowledgements

We thank the colleagues of East China Normal University and Fudan University for their help in collection of data and maintenance of eddy covariance systems. This work was founded by the National Natural Science Foundation of China (41871088 and 41977321), the National Key R&D Program of China (2017YFC0506001), and the project "Coping with deltas in transition" within the Programme of Strategic Scientific Alliances between China and The Netherlands (2016YFE0133700). This work was also supported by the Key Project of Shanghai Science and Technology Committee (19DZ2210200). We thank four anonymous reviewers for their constructive comments.

Appendix A. Supplementary data

Supplementary data to this article can be found online at https://doi.org/10.1016/j.scitotenv.2020.141214.

References

Abdul-Aziz, O.I., Ishtiaq, K.S., Tang, J., Moseman-Valtierra, S., Kroeger, K.D., Gonneea, M.E., Mora, J., Morkeski, K., 2018. Environmental controls, emergent scaling, and predictions of greenhouse gas (GHG) fluxes in coastal salt marshes. J. Geophys. Res.-Biogeo. 123, 2234–2256.

Barrett-Lennard, E.G., 2003. The interaction between waterlogging and salinity in higher plants: causes, consequences and implications. Plant Soil 253, 35–54.

Chmura, G.L., Anisfeld, S.C., Cahoon, D.R., Lynch, J.C., 2003. Global carbon sequestration in tidal, saline wetland soils. Global Biogeochem. Cy. 17, 1111.

Colmer, T.D., Greenway, H., 2005. Oxygen transport, respiration, and anaerobic carbohydrate catabolism in roots in flooded soils. In: Lambers, H., Ribas-Carbo, M. (Eds.), Plant respiration. Springer, Dordrecht, the Netherlands, pp. 137–158.

Davy, A.J., Brown, M.J., Mossman, H.L., Grant, A., 2011. Colonization of a newly developing salt marsh: disentangling independent effects of elevation and redox potential on halophytes. J. Ecol. 99, 1350–1357.

Ferguson, G., Gleeson, T., 2012. Vulnerability of coastal aquifers to groundwater use and climate change. Nat. Clim. Chang. 2, 342–345.

Forbrich, I., Giblin, A.E., 2015. Marsh-atmosphere CO_2 exchange in a New England salt marsh. J. Geophys. Res.-Biogeo. 120, 1825–1838.

Frankeberger, W.T., Johanson, J.B., 1983. Method of measuring invertase activity in soils. Plant Soil 74, 301–311.

Ge, Z., Cao, H., Cui, L., Zhao, B., Zhang, L., 2015. Future vegetation patterns and primary production in the coastal wetlands of East China under sea level rise, sediment reduction, and saltwater intrusion. J. Geophys. Res.-Biogeo. 120, 1923–1940.

Ge, Z., Li, S., Tan, L., Li, Y., Hu, Z., 2019. The importance of the propagule-sediment-tide "power balance" for revegetation at the coastal frontier. Ecol. Appl. 29, e01967.

Gleason, M.L., Dunn, E.L., 1982. Effects of hypoxia on root and shoot respiration of *Spartina alterniflora*. In: Kennedy, V.S. (Ed.), Estuarine comparisons. Academic Press, Gleneden Beach, OR, pp. 243–253.

Guo, H., Noormets, A., Zhao, B., Chen, J., Sun, G., Gu, Y., Li, B., Chen, J., 2009. Tidal effects on net ecosystem exchange of carbon in an estuarine wetland. Agric. For. Meteorol. 149, 1820–1828.

Hadas, A., Kautsky, L., Goek, M., Kara, E.E., 2004. Rates of decomposition of plant residues and available nitrogen in soil, related to residue composition through simulation of carbon and nitrogen turnover. Soil Biol. Biochem. 36, 255–266.

Halupa, P.J., Howes, B.L., 1995. Effects of tidally mediated litter moisture content on decomposition of *Spartina alterniflora* and *S. patens*. Mar. Biol. 123, 379–391.

Han, G., Chu, X., Xing, Q., Li, D., Yu, J., Luo, Y., Wang, G., Mao, P., Rafique, R., 2015. Effects of episodic flooding on the net ecosystem CO_2 exchange of a supratidal wetland in the Yellow River Delta. J. Geophys. Res.-Biogeo. 120, 1506–1520.

Han, X., Wang, D., Medeiros, S.C., Hagen, S.C., Hall, C.R., 2018. Assessing sea-level rise impact on saltwater intrusion into the root zone of a geo-typical area in coastal east-central Florida. Sci. Total Environ. 630, 211–221.

Heinsch, F.A., Heilman, J.L., McInnes, K.J., Cobos, D.R., Zuberer, D.A., Roelke, D.L., 2004. Carbon dioxide exchange in a high marsh on the Texas Gulf Coast: effects of freshwater availability. Agric. For. Meteorol. 125, 159–172.

Hu, Q., Wu, Q., Yao, B., Xu, X., 2015. Ecosystem respiration and its components from a Carex meadow of Poyang Lake during the drawdown period. Atmos. Environ. 100, 124–132.

Ikenaga, M., Guevara, R., Dean, A.L., Pisani, C., Boyer, J.N., 2010. Changes in community structure of sediment bacteria along the Florida coastal everglades marsh–mangrove–seagrass salinity gradient. Microb. Ecol. 59, 284–295.

Jones, S.F., Stagg, C.L., Krauss, K.W., Hester, M.W., 2018. Flooding alters plant-mediated carbon cycling independently of elevated atmospheric CO_2 concentrations. J. Geophys. Res.-Biogeo. 123, 1976–1987.

Kathilankal, J.C., Mozdzer, T.J., Fuentes, J.D., D'Odorico, P., McGlathery, K.J., Zieman, J.C., 2008. Tidal influences on carbon assimilation by a salt marsh. Environ. Res. Lett. 3, 044010.

Kirwan, M.L., Guntenspergen, G.R., 2012. Feedbacks between inundation, root production, and shoot growth in a rapidly submerging brackish marsh. J. Ecol. 100, 764–770.

Kirwan, M.L., Megonigal, J.P., 2013. Tidal wetland stability in the face of human impacts and sea-level rise. Nature 466, 96–99.

Knox, S.H., Windham-Myers, L., Anderson, F., Sturtevant, C., Bergamaschi, B., 2018. Direct and indirect effects of tides on ecosystem-scale CO_2 exchange in a brackish tidal marsh in Northern California. J. Geophys. Res.-Biogeo. 123, 787–806.

Koyro, H.W., 2006. Effect of salinity on growth, photosynthesis, water relations and solute composition of the potential cash crop halophyte *Plantago coronopus* (L.). Environ. Exp. Bot. 56, 136–146.

Krauss, K.W., Whitbeck, J.L., Howard, R.J., 2012. On the relative roles of hydrology, salinity, temperature, and root productivity in controlling soil respiration from coastal swamps (freshwater). Plant Soil 358, 265–274.

Krauss, K.W., Holm Jr., G.O., Perez, B.C., McWhorter, D.E., Cormier, N., Moss, R.F., Johnson, D.J., Neubauer, S.C., Raynie, R.C., 2016. Component greenhouse gas fluxes and radiative balance from two deltaic marshes in Louisiana: pairing chamber techniques and eddy covariance. J. Geophys. Res-Biogeo. 121, 1503–1521.

Kutzbach, L., Wagner, D., Pfeiffer, E.M., 2004. Effect of microrelief and vegetation on methane emission from wet polygonal tundra, Lena Delta, Northern Siberia. Biogeochemistry 69, 341–362.

Laura, R.D., 1977. Salinity and nitrogen mineralization in soil. Soil Biol. Biochem. 9, 333–336.

Li, S.H., Ge, Z.M., Xie, L.N., Chen, W., Yuan, L., Wang, D.Q., Li, X.Z., Zhang, L.Q., 2018a. Eco-physiological response of native and exotic salt marsh vegetation to waterlogging and salinity: implications for the effects of sea-level rise. Sci. Rep. 8, 2441.

Li, H., Dai, S., Ouyang, Z., Xie, X., Guo, H., Gu, C., Xiao, X., Ge, Z., Peng, C., Zhao, B., 2018b. Multi-scale temporal variation of methane flux and its controls in a subtropical tidal salt marsh in eastern China. Biogeochemistry 137, 163–179.

Liu, L., Wang, D., Chen, S., Yu, Z., Xu, Y., Li, Y., Ge, Z., Chen, Z., 2019. Methane emissions from estuarine coastal wetlands: implications for global change effect. Soil Sci. Soc. Am. J. 83, 1368–1377.

Lloyd, J., Taylor, J.A., 1994. On the temperature dependence of soil respiration. Funct. Ecol. 8, 315–323.

Lund, M., Lafleur, P.M., Roulet, N.T., Lindroth, A., Christensen, T.R., Aurela, M., Chojnicki, B.H., Flanagan, L.B., Humphreys, E.R., Laurilam, T., Oechel, W.C., Olejnik, J., Rinne, J.,

Schubert, P., Nilsson, M.B., 2010. Variability in exchange of CO_2 across 12 northern peatland and tundra sites. Glob. Chang. Biol. 16, 2436–2448.
Luo, M., Huang, J., Zhu, W., Tong, C., 2019. Impacts of increasing salinity and inundation on rates and pathways of organic carbon mineralization in tidal wetlands: a review. Hydrobiologia 827, 31–49.
Ma, A.N., Lu, J.J., 2011. Net ecosystem exchange of carbon and tidal effects in Chongxi wetland, Yangtze Estuary. Res. Environ. Sci. 24, 716–721 (in Chinese with English abstract).
Mcleod, E., Chmura, G.L., Bouillon, S., Salm, R., Björk, M., Duarte, C.M., Lovelock, C.E., Schlesinger, W.H., Silliman, B.R., 2011. A blueprint for blue carbon: toward an improved understanding of the role of vegetated coastal habitats in sequestering CO_2. Front. Ecol. Environ. 9, 552–560.
Möller, I., Kudella, M., Rupprecht, F., Spencer, T., Paul, M., van, W.B.K., Wolters, G., Jensen, K., Bouma, T.J., Miranda-Lange, M., Schimmels, S., 2014. Wave attenuation over coastal salt marshes under storm surge conditions. Nat. Geosci. 7, 727–731.
Morison, J.I.L., Piedade, M.T.F., Müller, E., Long, S.P., Junk, W.J., Jones, M.B., 2000. Very high productivity of the C_4 aquatic grass *Echinochloa polystachya* in the Amazon floodplain confirmed by net ecosystem CO_2 flux measurements. Oecologia 125, 400–411.
Morrissey, E.M., Gillespie, J.L., Morina, J.C., Franklin, R.B., 2014. Salinity affects microbial activity and soil organic matter content in tidal wetlands. Glob. Chang. Biol. 20, 1351–1362.
Neubauer, S.C., 2013. Ecosystem responses of a tidal freshwater marsh experiencing saltwater intrusion and altered hydrology. Estuar. Coast. 36, 491–507.
Neubauer, S.C., Franklin, R.B., Berrier, D.J., 2013. Saltwater intrusion into tidal freshwater marshes alters the biogeochemical processing of organic carbon. Biogeosciences 10, 8171–8183.
Pagter, M., Bragato, C., Malagoli, M., Brix, H., 2009. Osmotic and ionic effects of NaCl and Na_2SO_4 salinity on *Phragmites australis*. Aquat. Bot. 90, 43–51.
Pennings, S.C., Callaway, R.M., 1992. Salt marsh plant zonation: the relative importance of competition and physical factors. Ecology 73, 681–690.
Pezeshki, S.R., 2001. Wetland plant responses to soil flooding. Environ. Exp. Bot. 46, 299–312.
Pulford, I.D., Tabatabai, M.A., 1988. Effect of waterlogging on enzyme activities in soils. Soil Biol. Biochem. 20, 215–219.
Rath, K.M., Rousk, J., 2015. Salt effects on the soil microbial decomposer community and their role in organic carbon cycling: a review. Soil Biol. Biochem. 81, 108–123.
Schuerch, M., Spencer, T., Temmerman, S., Kirwan, M.L., Wolff, C., Lincke, D., McOwen, C.J., Pickering, M.D., Reef, R., Vafeidis, A.T., Hinkel, J., Nicholls, R.J., Brown, S., 2018. Future response of global coastal wetlands to sea-level rise. Nature 561, 231–234.
Schwarz, M., Gale, J., 1981. Maintenance respiration and carbon balance of plants at low levels of sodium chloride salinity. J. Exp. Bot. 32, 933–941.
Spalding, E.A., Hester, M.W., 2007. Interactive effects of hydrology and salinity on oligohaline plant species productivity: implications of relative sea-level rise. Estuar. Coast. 30, 214–225.
State Oceanic Administration (People"s Republic of China), 2012. Bulletin of Chinese marine environment. on. http://www.nmdis.org.cn/hygb/zghyhjzlgb/2012nzghyhjzkgb/.
State Oceanic Administration (People"s Republic of China), 2018. Bulletin of Chinese sea level rise. on. http://gi.mnr.gov.cn/201905/t20190510_2411195.html.
Sudhir, P., Murthy, S.D.S., 2004. Effects of salt stress on basic processes of photosynthesis. Photosynthetica 42, 481–486.
Tan, L., Ge, Z., Zhou, X., Li, S., Li, X., Tang, J., 2020. Conversion of coastal wetlands, riparian wetlands and peatlands increases greenhouse gas emissions: a global metaanalysis. Glob. Chang. Biol. 26, 1638–1653.
Thornley, J.H.M., 1998. Dynamic model of leaf photosynthesis with acclimation to light and nitrogen. Ann. Bot. 81, 421–430.
Tripathi, S., Chakraborty, A., Chakrabarti, K., Bandyopadhyay, B.K., 2007. Enzyme activities and microbial biomass in coastal soils of India. Soil Biol. Biochem. 39, 2840–2848.
Vance, E.D., Brookes, P.C., Jenkinson, D.S., 1987. An extraction method for measuring soil microbial biomass C. Soil Biol. Biochem. 19, 703–707.
Wang, F., Lu, X., Sanders, C.J., Tang, J., 2019. Tidal wetland resilience to sea level rise increases their carbon sequestration capacity in United States. Nat. Commun. 10, 5434.
Weston, N.B., Neubauer, S.C., Velinsky, D.J., Vile, M.A., 2014. Net ecosystem carbon exchange and the greenhouse gas balance of tidal marshes along an estuarine salinity gradient. Biogeochemistry 120, 163–189.
Wilson, B.J., Mortazavi, B., Kiene, R.P., 2015. Spatial and temporal variability in carbon dioxide and methane exchange at three coastal marshes along a salinity gradient in a northern Gulf of Mexico estuary. Biogeochemistry 123, 329–347.
Wilson, B.J., Servais, S., Charles, S.P., Davis, S.E., Gaiser, E.E., Kominoski, J.S., Richards, J.H., Troxler, T.G., 2018a. Declines in plant productivity drive carbon loss from brackish coastal wetland mesocosms exposed to saltwater intrusion. Estuar. Coast. 41, 2147–2158.
Wilson, B.J., Servais, S., Mazzei, V., Kominoski, J.S., Hu, M., Davis, S.E., Gaiser, E., Sklar, F., Bauman, L., Kelly, S., Madden, C., Richards, J., Rudnick, D., Stachelek, J., Troxler, T.G., 2018b. Salinity pulses interact with seasonal dry-down to increase ecosystem carbon loss in marshes of the Florida Everglades. Ecol. Appl. 28, 2092–2108.
Zhang, Y., Li, C., Trettin, C.C., Li, H., Sun, G., 2002. An integrated model of soil, hydrology, and vegetation for carbon dynamics in wetland ecosystems. Global. Biogeochem. Cy. 16, 1–17.
Zhao, J., Malone, S.L., Oberbauer, S.F., Olivas, P.C., Schedlbauer, J.L., Staudhammer, C.L., Starr, G., 2019. Intensified inundation shifts a freshwater wetland from a CO_2 sink to a source. Glob. Chang. Biol. 25, 3319–3333.